Geometrical tuning of thermal phonon spectrum in nanoribbons

2016 J. Phys. D: Appl. Phys. 49 115306

(http://iopscience.iop.org/0022-3727/49/11/115306)

IOP Publishing Journal of Physics D: Applied Physics
J. Phys. D: Appl. Phys. **49** (2016) 115306 (8pp) doi:10.1088/0022-3727/49/11/115306

Geometrical tuning of thermal phonon spectrum in nanoribbons

Aymeric Ramiere[1,3], Sebastian Volz[2] and Jay Amrit[1]

[1] Laboratoire d'Informatique pour la Mécanique et les Sciences de l'Ingénieur, LIMSI-CNRS UPR 3251, Université Paris Sud, Rue John von Neumann, 91403 Orsay, France
[2] Laboratoire Énergétique Moléculaire et Macroscopique Combustion, EM2C-CNRS UPR 288, École Centrale Paris, Grande voie des Vignes, 92295 Chatenay-Malabry, France

E-mail: jay.amrit@limsi.fr

Received 23 November 2015, revised 10 January 2016
Accepted for publication 18 January 2016
Published 17 February 2016

Abstract

Phonon spectral energy transmission in silicon nanoribbons is investigated using Monte-Carlo simulations in the boundary scattering regime by changing the length and width geometrical parameters. We show that the transition frequency from specular scattering to diffuse scattering is inversely proportional to the edge roughness σ with a geometry independent factor of proportionality. The increase of the length over width ratio ζ leads to a decrease of the energy transmission in the diffuse scattering regime which evolves as $(1+\zeta^{0.59})^{-1}$. This trend is explained by developing a model of phonon energy transmission in the fully diffuse scattering regime which takes into account the probability for a diffusively scattered phonon to be directly transmitted from any position on the edge of the nanoribbon. This model establishes the importance of the solid angles in the energy transmission evolution with ζ. The transition from unity energy transmission in the specular scattering regime to reduced transmission in the diffuse scattering regime constitutes a low-pass frequency filter for phonons. Our simulations show an energy rejection rate better than 90% for high ζ, which paves the way for potential high performance filters. Filtering out high frequency phonons is of significant interest for phononic crystal applications, which use band engineering of phonons in the wave regime with low frequencies.

Keywords: phonons, spectrum, roughness, Monte-Carlo

(Some figures may appear in colour only in the online journal)

Introduction

The influence of surface roughness on heat transport has emerged over the past decade as being crucial in affecting the thermal conduction in materials [1, 2]. Many experimental studies have demonstrated that surface roughness significantly reduces thermal conductivity in silicon nanowires [3–10]. In parallel, the rise of 2D materials and measurements of the thermal properties of graphene also highlighted the important role of edge roughness on nanoribbons [11, 12].

A clear understanding of phonon scattering at boundaries requires the surface state to be characterized. The morphology of a surface is generally defined by the root mean square height distribution σ, also called roughness, and the characteristic roughness correlation dimension l. These parameters are generally determined from the Fourier transform of the autocorrelation function of the surface profile. Although these aspects were mentioned earlier by Lim *et al* [9] and Ghossub *et al* [6], it is only very recently that Maurer *et al* [13] have studied numerically the effect of the correlation length on the thermal conductivity and have shown that decreasing the correlation length suppresses the thermal conductivity.

Experimentally, nanowires with rectangular cross sections or nanoribbons are cut out from a large membrane using an electron beam. The original membrane is almost atomically flat while the electron beam induces an edge roughness

[3] Author to whom any correspondence should be addressed.
Present address: LIMMS-CNRS/IIS-University of Tokyo, UMI CNRS 2820, 4-6-1 Komaba, Meguro-ku 153-8505 Tokyo, Japan.

of a few nanometers (see inset of figure 2) with a correlation length of the order of 100 nm [10, 14].

Several simulation methods have been used to investigate the impact of the roughness of phonon transport such as Green functions [15], phonon hydrodynamics [16], perturbation theory [17], wave packets [18] and the Boltzmann transport equation (BTE) [19–22]. Concerning the latter, the Monte-Carlo (MC) technique is often used to solve the BTE considering phonons as particles moving inside the nanostructure [13, 19, 23–28]. Klitsner *et al* [29] were the first to use the MC technique to simulate phonon transport in the boundary scattering regime (BSR) assuming a monochromatic phonon source and an arbitrary factor of specularity. More recently, Lacroix *et al* [25] have underlined the importance of boundary scattering but their MC simulations are mainly carried out near room temperature where internal phonon–phonon processes dominate heat transport.

Up to now applications of thermal nanodevices have mainly been dedicated to thermal management of electronics [30] and thermoelectric modules [31, 32]. In this work we propose a new application which is a tunable low-pass phonon filter that becomes possible by controlling the geometry and the edge roughness of nanoribbons.

We simulate phonon–surface roughness interactions in nanoribbons using the MC technique to examine the spectral energy transmission as a function of the length over width ratio ζ. On the the one hand, we present evidence that diffuse scattering at surface boundaries enables the filtering of phonons above a cut-off frequency that depends on the root mean square (rms) surface roughness σ and on ζ. On the other hand, we show that the higher ζ, the more high frequency phonons are attenuated, improving the filter performance.

Boundary scattering regime

In our model, phonon–boundary interaction is considered to be the only scattering mechanism occurring in the nanoribbon. This BSR is known to be applicable at low temperature because internal processes are proportional to power laws of the temperature [33]. Nevertheless, we can show that miniaturization of the devices inevitably leads to an increase of the number of interactions with the boundaries that can prevail over phonon–phonon processes even at room temperature.

Three main phonon scattering mechanisms occur in a crystal: impurity scattering with a relaxation time τ_i, boundary scattering with τ_B and phonon–phonon (p–p) processes with τ_{p-p}. The total phonon relaxation time τ_T is determined using Matthiesen's rule

$$\tau_T^{-1} = \tau_i^{-1} + \tau_B^{-1} + \tau_{p-p}^{-1} \quad (1)$$

In this expression p–p processes include both Normal and Umklapp scattering. We consider the crystal to be almost defect free so that the impurity term in equation (1) can be neglected. Therefore, there is a competition between p–p processes and boundary scattering.

In order to neglect p–p processes with respect to boundary scattering we consider that the following condition must be satisfied

$$\tau_B \leqslant 10\tau_{p-p} \quad (2)$$

The boundary scattering relaxation time is estimated at $\tau_B^{-1} = v_g/d$ where v_g is the group velocity and d the characteristic dimension, which is the width or thickness in a rectangular geometry. For numerical application, the most common material for electronic applications is silicon with $v_g = 5930\,\mathrm{m\,s^{-1}}$ [34]. The relaxation times associated with the p–p processes are calculated using Holland's expressions [27, 33] for longitudinal and transverse modes. These relaxation times depend on the temperature and the phonon frequency. For a system at a temperature T, a Planck-like frequency distribution is associated but is generally not accessible experimentally. A global behavior of this distribution is deduced by considering the frequency that contributes the most to the energy distribution. This definition leads to the dominant phonon wavelength $\lambda_{dom} = hv_g/(2.82k_BT)$ [7, 35]. Consequently, the inequality of equation (2) defines the upper limit of the dimension d_{p-p} above which the p–p interactions have to be taken into account at a given temperature.

At the opposite end, a lower limit of the dimension also exists under which the BSR disappears. Indeed, as the temperature and/or the characteristic dimension decreases, the wavelength of phonons becomes comparable to d, leading to the onset of phonon confinement. In this case, the wave nature of phonons has to be taken into account. A treatment of the latter is not within the scope of the present study. It defines the lower dimension $d_{conf} = \lambda_{dom}$ to avoid the confinement effects and to ensure that BSR is valid.

Figure 1 shows the BSR area, limited by d_{p-p} and d_{conf} represented with the solid red line and solid blue line respectively, as a function of the characteristic dimension of the system and the temperature. We have limited the lowest temperature to 10 mK, which is accessible with a dilution refrigerator and the smallest dimension to 5 nm that is the fabrication limit today. We observe that the BSR, represented by the hatched area, forms a cone that enlarges when temperature decreases. Under ~40 K the BSR is always predominant over other processes in a microwire even when d is larger than 10 μm. As T increases and d decreases the boundary scattering cones shrink to reach 210 K for $d_{conf} = 5$ nm.

The hatched area in figure 1 is the ideal zone to observe the effects of the BSR where other scattering processes can be ignored. In the proximity of the boundary limits of this area, the BSR still has a strong impact. Indeed, we can relax equation (2) with the equality $\tau_B = \tau_{p-p}$ to obtain d^*_{p-p} represented with the red dashed line in figure 1. Between d_{p-p} and d^*_{p-p} boundary scattering remains the main scattering mechanism but is progressively weakened as the p–p processes appear. The condition on the confinement effect can also be relaxed since Heron *et al* [7] observed no wave effects in silicon nanowires of 100 nm down to 0.3 K where $\lambda_{dom} = 340$ nm. Thus, we can consider that the BSR is still present when $d < 10\lambda_{dom}$ which

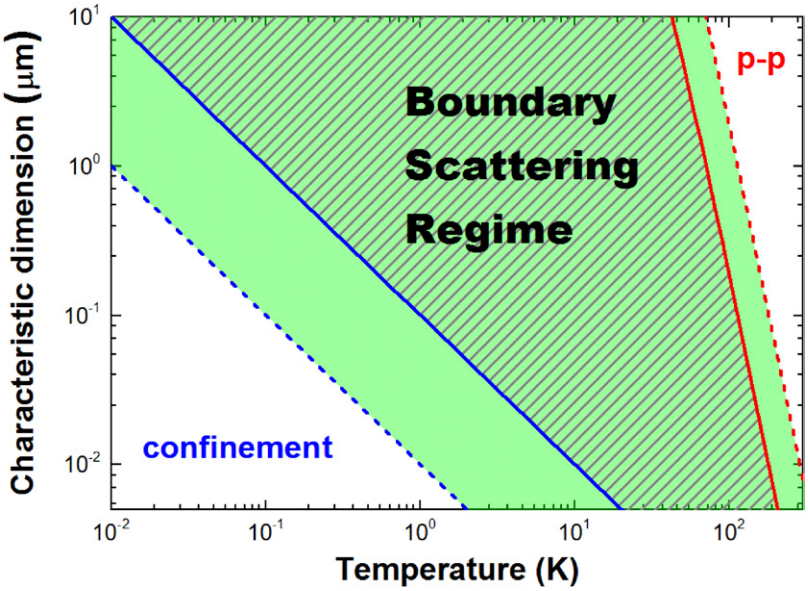

Figure 1. Heat transfer regimes depending on the characteristic dimension and the temperature. Solid red line: $d_{\text{p–p}}$, defines the upper limit of BSR above which p–p processes are not negligible. Dashed red line: $d^*_{\text{p–p}}$, equilibrium between boundary scattering and p–p processes. Solid blue line: d_{conf}, lower limit of the BSR below which confinement effects appear. Dashed blue line: d^*_{conf}, relaxed condition for confinement effects. Green area: area where boundary scattering dominates. Hatched area: optimum area for filter applications.

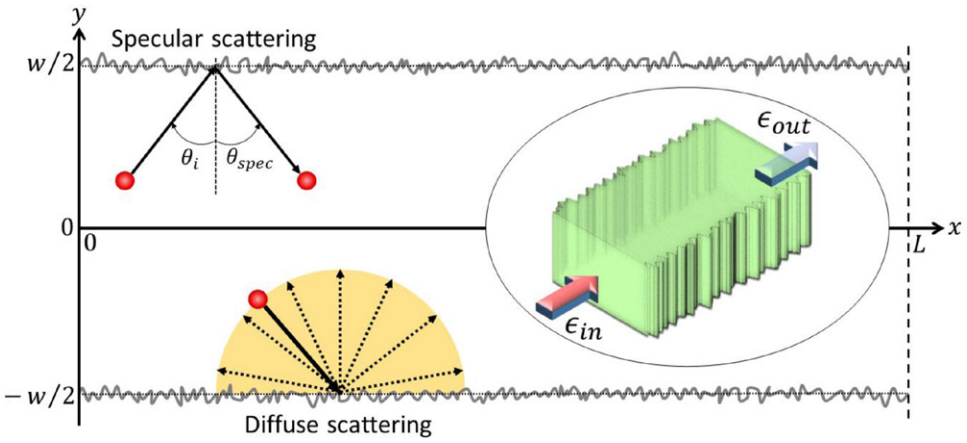

Figure 2. Schematic of the studied nanoribbon.

is represented by d^*_{conf} with the blue dashed line in figure 1. The two relaxed conditions, $d^*_{\text{p–p}}$ and d^*_{conf} define a larger cone for the BSR, depicted by the green area, that contains the room temperature for dimensions smaller than 10 nm.

The BSR represent the context of this study. We have shown that its range of existence is relatively broad and has therefore a practical interest for applications. In the rest of the paper we suppose that we are in the BSR.

Monte-Carlo method

We use a homemade MC code to simulate phonon transport in rectangular cross-sectional nanowires with smooth top and bottom surfaces and rough lateral surfaces (see inset of figure 2). From the energy transmission point of view this situation is equivalent to a 2D nanoribbon. Therefore, we simulate phonons only in the 2D (x; y) frame of reference.

At the beginning of the simulation, all phonons are situated at the nanoribbon's entrance $x_0 = 0$ (see figure 2). For each phonon, y_0 is taken randomly in the $[-w/2; w/2]$ interval and the initial direction θ_0 is also picked randomly in the half space within the nanoribbon. Then, the phonon moves ballistically inside the nanoribbon interacting only with the boundaries until it either reaches $x = L$, where it is counted as transmitted, or it goes back to $x = 0$ and is considered as backscattered.

The scattering mechanism at the boundary surfaces is quantified with the aid of the specularity probability parameter p_{S} as defined by Soffer [36]. This model is a generalization of Ziman's specularity parameter [37] that takes into account all impinging angles on the rough surface. It is assumed that the phonon wavelength λ is much bigger than the correlation length and that the rms surface roughness σ is smaller than λ [38]. These two conditions are also called randomly rough

surface and weakly rough surface respectively. They define an analytical expression for the specularity parameter given by

$$p_S = \exp\left(-16\pi^2 \frac{\sigma^2}{\lambda^2} \cos^2\theta_i\right) \quad (3)$$

where θ_i is the angle of the incoming phonon relative to the normal of the average plane. The roughness is an input parameter and $\lambda = 2\pi v_g/\omega$ where $v_g = 5930\,\mathrm{m\,s^{-1}}$ is identical for all the phonons. When a phonon is scattered on a geometrical boundary two distinct outcomes can happen: specular scattering, which conserves the incident angle, or diffuse scattering where the phonon completely loses the information of its previous trajectory and scatters into an arbitrary direction within the medium as depicted by the half circle in figure 2. In order to select the outcome, a random number η is picked between 0 and 1. If $\eta \leqslant p_S$, the phonon undergoes a specular scattering otherwise it is diffusively scattered. In this latter case, a second random number θ_{diff}, representing the diffused phonon angle, is uniformly picked within the half space of the nanoribbon [24].

As we study the phonon spectral transmission, we sweep the angular frequency over six orders of magnitudes from 0.1 GHz to 70 THz to cover temperatures ranging from millikelvins to room temperature. The 70 THz upper limit is given by the size of the silicon unit cell that defines the minimum wavelength. For each angular frequency ω we launch $N_{in} = 10^6$ phonons at the entrance of the nanoribbon adding up to an input energy $\epsilon_{in} = \sum_{in} \hbar\omega$. Then, we assess the energy at the output of the nanoribbon $\epsilon_{out} = \sum_{out} \hbar\omega$. The energy transmission is given by [39]:

$$\Gamma_\epsilon(\omega) = \frac{\sum_{out} \hbar\omega}{\sum_{in} \hbar\omega} = \frac{N_{out}(\omega)}{N_{in}(\omega)} \quad (4)$$

In the BSR the phonons can only modify their energy at the boundaries. We suppose that radiations are negligible before conduction and that the nanoribbon is in the vacuum. Moreover, we assume that phonons do not split up under the scattering process so that one impinging phonon leaves the rough surface also as one phonon. Therefore, the phonons conserve their frequency at all times and the energy transmission becomes the ratio of the number of phonons going out over the phonons coming in. The large number of phonons N_{in} ensures robust statistics and low noise in our results.

Results and discussions

In figure 3(a), we plot the energy transmission $\Gamma_\epsilon(\omega)$ for different values of the roughness between 0.5 nm and 20 nm for a constant ratio of length over average width $\zeta = L/w = 4$. All the curves show the same trends with almost unity transmission for the lowest frequencies that decreases rapidly to reach a minimum plateau at high frequencies. The nearly unity transmission is explained by the large predominance of the specular scattering at the boundaries and defines the specular scattering regime. The increase of diffuse scattering events logically decreases the energy transmission. For high frequencies, all phonons are diffusively scattered, leading to the observed minimum plateau and corresponding to the diffuse scattering regime. The transition from the specular scattering regime to the diffuse scattering regime is characterized by the scattering cut-off frequency ω_{scat} that we define with the expression:

$$\Gamma_\epsilon(\omega_{scat}) = \frac{\Gamma_{spec} + \Gamma_{diff}}{2} \quad (5)$$

where Γ_{spec} is the specular transmission equal to 1 by definition, and Γ_{diff} is the transmission in the diffuse scattering regime. In the case $\zeta = 4$, we see in figure 3(a) that $\Gamma_{diff} = 0.38$ so that ω_{scat} is obtained for $\Gamma_\epsilon = 0.72$. We observe that the higher the roughness, the lower ω_{scat} reflecting the properties of equation (3). Our simulations give more insights of this phenomenon as displayed in figure 2(b) which shows that ω_{scat} is inversely proportional to the roughness. Now, we can write $\omega_{scat} = A/\sigma$ and we find $A = 2.0\,\mathrm{THz\,nm}$. This coefficient A tells us that changing the roughness by 1 nm leads to a shift of 2 THz in the scattering cut-off frequency.

The rapid transition from specular scattering to the diffuse scattering leads to the interesting concept of phonon frequency filtering. By analogy with sound, we define an attenuation of the phonon energy intensity as:

$$\alpha(\omega) = -10 \log \Gamma_\epsilon(\omega) \quad (6)$$

A standard criterion to obtain a filter is that the attenuation must be superior to 3 dB [40]. It also corresponds to 50% of signal rejection. Therefore we define the filter cut-off frequency ω_{filt} at $\Gamma_\epsilon(\omega_{filt}) = 0.5$. Figure 3(b) shows that, as for the scattering cut-off frequency, we obtain a linear dependence between the filter cut-off frequency and the inverse of the roughness, that is $\omega_{filt} = B/\sigma$ with $B = 5.8\,\mathrm{THz\,nm}$. This observation offers the possibility of precise control on the filter cut-off frequency by nanoengineering the edge roughness.

Figure 4 shows $\Gamma_\epsilon(\omega)$ for various ζ ranging from 1 to 50 while the roughness is held constant at 4 nm. The transmission in the specular scattering regime remains equal to unity but the diffuse scattering regime Γ_{diff} becomes smaller as ζ increases. We also notice that the transition region expands with increasing ζ so it progressively pushes the specular scattering regime to lower frequencies and the diffuse scattering regime to higher frequencies. Consequently, the filter cut-off frequency ω_{filt} decreases with the increase of ζ. These behaviours can be explained by the increase of the number of interactions between a phonon and the boundaries with the increase of ζ. Indeed, more scattering events increase the probability for the phonons to be diffusively scattered, thereby reducing the range of the specular scattering regime and lowering Γ_{diff}.

In the fully established diffuse scattering regime, the diminution of Γ_{diff} with ζ is quantified in figure 5(a). As we are mostly interested in the filtering capacities of the nanoribbons, we convert the energy transmission Γ_{diff} into attenuation α_{diff} using equation (6). The 3 dB limit, to characterize the nanoribbon as an effective filter, is exceeded for $\zeta > 2$. The filter efficiency increases as ζ increases and it goes beyond

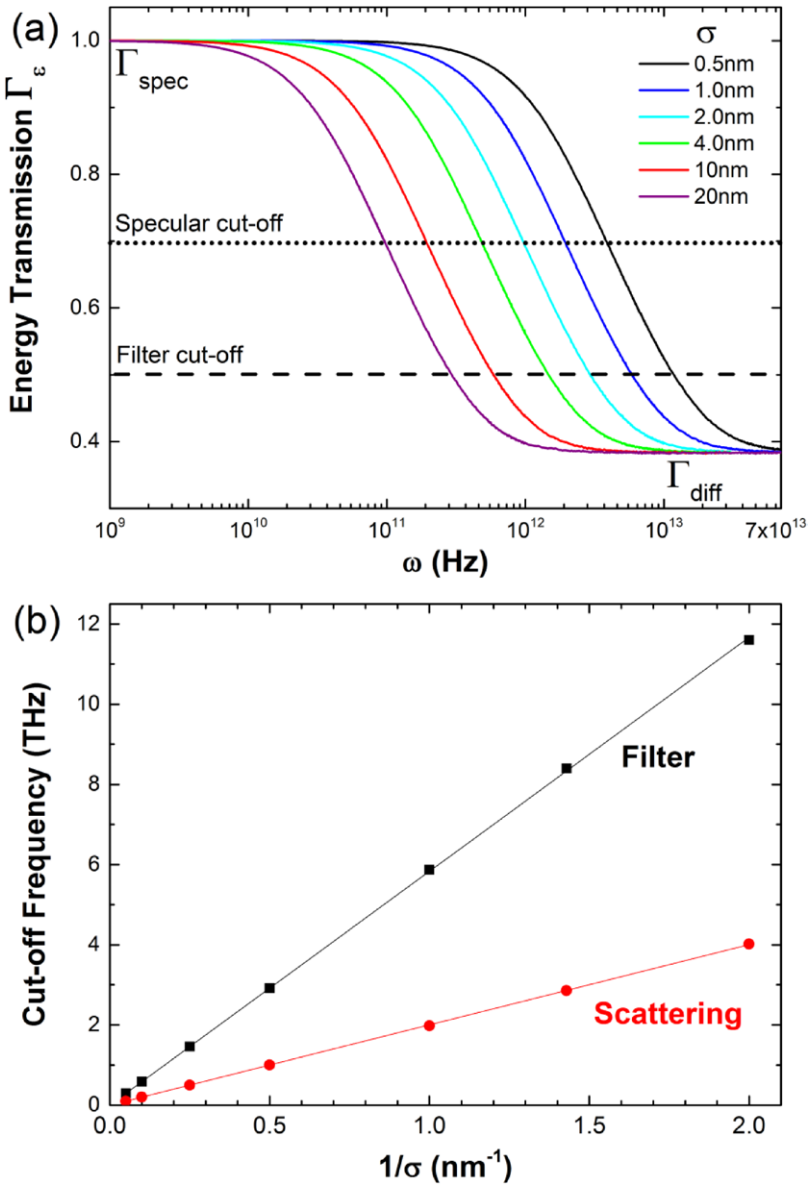

Figure 3. Impact of surface roughness for $\zeta = L/w = 4$. (a) Monte-Carlo simulations of the spectral energy transmission for roughnesses between 0.5 nm and 20 nm. Dashed line: cut-off frequency for filter applications. Dotted line: cut-off frequency for transition between specular scattering and diffuse scattering. (b) Evolution of the two cut-off frequencies as a function of the inverse of the roughness.

10 dB (90% of rejection) for $\zeta > 80$. This value is completely reasonable since silicon nanowires with ζ exceeding 200 are commonly fabricated [3, 8, 14, 31]. For the practical purpose of calculating the maximum attenuation, our MC simulations can be fitted by the power law curve $\Gamma_{diff}(\zeta) = (1 + \zeta^{0.59})^{-1}$.

In order to give a physical explanation to our MC points (black dots) in figure 5(a), we develop here a theory on the phonon transport in the fully diffuse scattering regime. Inherent to our simulations, we can distinguish two kinds of phonons: the first are phonons that cross the nanoribbon without interacting with its boundaries and the second are phonons that undergo at least one scattering event (necessarily diffuse since we are in the fully diffuse BSR). They are noted Γ_{cross} and Γ_{scat} respectively. These two contributions are complementary so that we can write

$$\Gamma_{diff}(\zeta) = \Gamma_{cross}(\zeta) + \Gamma_{scat}(\zeta) \tag{7}$$

We theoretically determine these two terms by considering their solid angles with respect to the entrance ($x = 0$) and the output ($x = L$) of the nanoribbon. A phonon at the entrance of the nanoribbon sees the output with a solid angle Ω_{cross} (see inset of figure 5(a)). Statistically, the average initial position of the phonons is at the midpoint $y = 0$, so we have $\Omega_{cross} = \arctan[w/(2L)]$. This solid angle is then normalized to obtain the crossing energy transmission:

$$\Gamma_{cross}(\zeta) = \frac{2}{\pi}\arctan\left(\frac{1}{2\zeta}\right) \tag{8}$$

Equation (8) is plotted with the red curve in figure 5(a). For $\zeta < 1$ our model of phonons crossing the nanoribbon is in

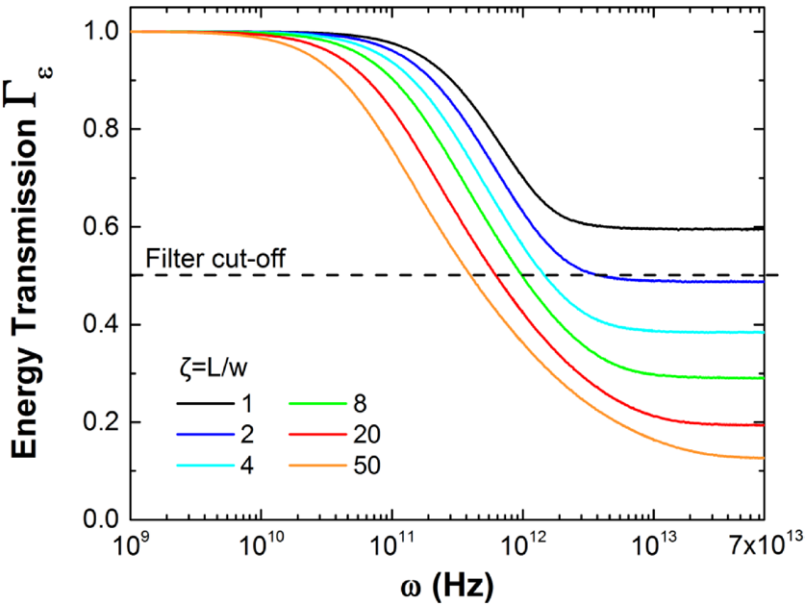

Figure 4. Monte-Carlo simulations of the spectral energy transmission for different ζ from 1 to 50 with $\sigma = 4$ nm. The filter is effective for $\Gamma_\epsilon < 0.5$ represented by the dashed line.

very good agreement with the simulation results. But, Γ_{cross} decreases very rapidly and becomes negligible for $\zeta > 10$.

For a phonon being scattered at any position x on a boundary of the nanoribbon, we define two solid angles $\Omega_{in}(x)$ and $\Omega_{out}(x)$. $\Omega_{in}(x)$ is the solid angle corresponding to the entrance of the nanoribbon as seen by the phonon at the scattering position x. Reciprocally, $\Omega_{out}(x)$ is the solid angle corresponding to the output of the nanoribbon as seen by the phonon at position x. As the scattering regime is fully diffusive, when a phonon is scattered on a boundary, it has the same chance to go in any direction in the half space within the nanoribbon. Therefore, the probability for a phonon to go directly, i.e.without being scattered anymore, to the entrance from its scattering location is proportional to $\Omega_{in}(x)$. On the other hand, its probability to be directly transmitted is proportional to $\Omega_{out}(x)$. A simple geometrical analysis gives $\Omega_{out}(x) = \arctan[w/(L-x)]$. Taking into account all possible scattering locations leads to the integral $\Gamma_{scat}(\zeta) \propto \int \Omega_{out}(x)dx \propto [\zeta \arctan(1/\zeta) + \ln(1+\zeta^2)/2]$. From a strict mathematical point of view, this integral should depend on both x and width w but it cannot be calculated analytically. This difficulty can be overcome if we consider a constant width that will only introduce a shift in Γ_{scat} that can be incorporated in the integral constants. As a result, we obtain finally:

$$\Gamma_{scat}(\zeta) = C\zeta \arctan\left(\frac{1}{\zeta}\right) + \frac{D}{2}\ln(1+\zeta^2) \qquad (9)$$

where C and D are the constants to be determined. The arctan term in this expression represents the increase of the energy transmission thanks to the scattering events that are now taken into account. This term quickly saturates to reach a plateau as each time a phonon is scattered it can be reflected in any direction. In contrast, the logarithm term accounts for the backscattering that reduces the energy transmission.

The coefficients were deduced by fitting the curve $\Gamma_{diff}(\zeta) - \Gamma_{cross}(\zeta)$ as written in equation (7) and we find $C = 0.40$ and $D = -0.07$. Using these values, $\Gamma_{scat}(\zeta)$ is represented in figure 5(a) with the blue line. At the origin, as no edges are present so all phonons cross the nanoribbon directly, we have $\Gamma_{scat}(\zeta = 0) = 0$. By increasing ζ, Γ_{scat} also increases because phonons are transmitted after being scattered as explained above. Γ_{scat} reaches Γ_{cross} for $\zeta \approx 1$ and continues to increase to reach a maximum at $\zeta \approx 2$ where Γ_{cross} and Γ_{scat} account for 1/3 and 2/3 respectively of the diffusive energy transmission Γ_{diff}. For $\zeta > 2$, Γ_{scat} decreases to finally give the decreasing tendency of Γ_{diff} for high ζ. Finally, we sum Γ_{cross} and Γ_{scat} as we have calculated to obtain the black dashed curve in figure 5(a). We observe that the theoretical curve is in very good agreement with the black points of the MC simulations.

Physically, the behavior at high ζ can be understood with the two solid angles previously defined, namely $\Omega_{in}(x)$ and $\Omega_{out}(x)$. Logically, as long as the phonon is in the first half of the nanoribbon ($x < L/2$) we have $\Omega_{in}(x) > \Omega_{out}(x)$, so it has a higher probability to be backscattered than transmitted. In contrast, when the scattering event occurs in the second half of the length, the phonon has a greater chance to be transmitted. But there are less phonons available in the latter case because a portion of the phonons has already been backscattered. Consequently, the final outcome is that the increase of ζ reduces the transmitted energy in the fully diffuse scattering regime.

Figure 5(b) shows the evolution of the two cut-off frequencies ω_{scat} and ω_{filt} as a function of ζ for a constant roughness $\sigma = 4$ nm. The filter cut-off frequency ω_{filt} shifts to lower frequencies by ~85% as ζ is increased from 2 to 30. On the other hand, the specular to diffuse scattering transition frequency ω_{scat} decreases by ~40% in the same ζ range. As ζ increases, Γ_{diff} tends to zero so the two cut-off frequencies are slowly converging to zero.

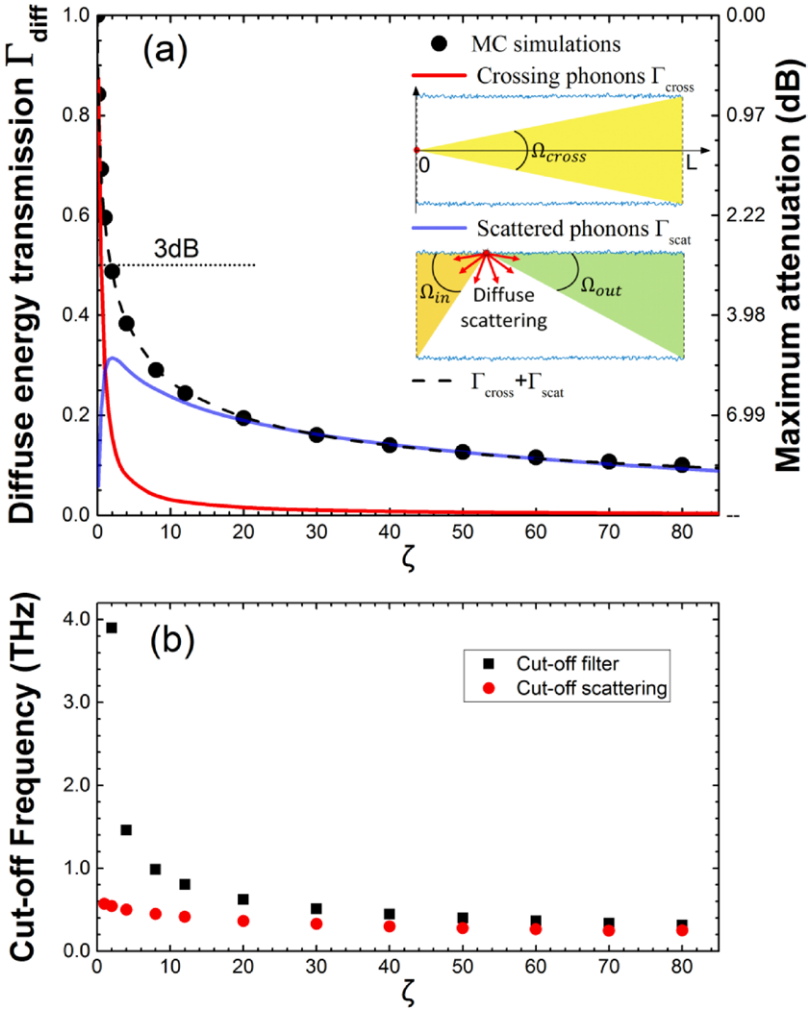

Figure 5. Impact of ζ in the diffuse scattering regime for $\sigma = 4$ nm. (a) Monte-Carlo simulations of the diffuse energy transmission Γ_{diff} (black dots). Red line: transmission of phonons crossing the nanoribbon without interacting with boundaries (equation (8)). Blue line: transmission of diffusely scattered phonons at boundaries (equation (9)). (b) Cut-off frequencies for filter (black squares) and boundary scattering (red circles).

The linear dependence of the cut-off frequency as a function of the inverse of the roughness, as shown in figure 2(b), can be found for all length over width ratios ζ. As a result, the slope can be determined knowing one single cut-off frequency for a given ζ. Therefore, by multiplying the cut-off frequencies plotted in figure 4(b) with the roughness, which is here equal to 4 nm, we obtain the coefficients A and B for any dimension ζ.

Conclusion

We have examined the role of geometry and surface roughness when boundary scattering is predominant during phonon energy transmission in nanoribbons. Our analysis goes beyond confirming the intuitively accepted tendency that transmission decreases with length. We have shown that the transition frequency ω_{scat} from specular to diffuse scattering varies as the inverse of the rms surface roughness σ for a nanoribbon of a given L/w ratio. Further, we have demonstrated that an important phonon filtering effect is present. The latter is characterized by a cut-off frequency ω_{filt}, which is also proportional to $1/\sigma$. Moreover, our results show that it is possible to control these cut-off frequencies and attenuation by engineering σ and L/w. We have established a theory that successfully describes the energy transmission in the fully diffuse scattering regime. Recently, Alaie *et al* [41] reported measurements of coherent phonon scattering at room temperature in 2D phononic crystals. They showed that deviation from the incoherent scattering is low because only long wavelength phonons are affected by the crystal periodicity and these phonons represent only a few percent of the total spectrum. We believe that this effect can be strongly enhanced by introducing a low-pass phonon filter as we have demonstrated. Further studies are being conducted with different geometries in order to reject low frequency phonons and obtain a band-pass filter.

Acknowledgments

This work was initiated as part of a project supported by the LabEx LaSIPS, Paris-Saclay University.

References

[1] Cahill D G *et al* 2014 Nanoscale thermal transport. II. 2003–2012 *Appl. Phys. Rev.* **1** 11305

[2] Yang N, Xu X, Zhang G and Li B 2012 Thermal transport in nanostructures *AIP Adv.* **2** 41410

[3] Chen R, Hochbaum A I, Murphy P, Moore J, Yang P and Majumdar A 2008 Thermal conductance of thin silicon nanowires *Phys. Rev. Lett.* **101** 105501

[4] Hochbaum A I, Chen R, Delgado R D, Liang W, Garnett E C, Najarian M, Majumdar A and Yang P 2008 Enhanced thermoelectric performance of rough silicon nanowires *Nature* **451** 163–7

[5] Fon W, Schwab K, Worlock J and Roukes M 2002 Phonon scattering mechanisms in suspended nanostructures from 4 to 40 K *Phys. Rev.* B **66** 45302

[6] Ghossoub M G, Valavala K V, Seong M, Azeredo B, Hsu K, Sadhu J S, Singh P K and Sinha S 2013 Spectral phonon scattering from sub-10 nm surface roughness wavelengths in metal-assisted chemically etched Si nanowires *Nano Lett.* **13** 1564–71

[7] Heron J S, Fournier T, Mingo N and Bourgeois O 2009 Mesoscopic size effects on the thermal conductance of silicon nanowire *Nano Lett.* **9** 1861–5

[8] Li D, Wu Y, Kim P, Shi L, Yang P and Majumdar A 2003 Thermal conductivity of individual silicon nanowires *Appl. Phys. Lett.* **83** 2934–6

[9] Lim J, Hippalgaonkar K, Andrews S C, Majumdar A and Yang P 2012 Quantifying surface roughness effects on phonon transport in silicon nanowires *Nano Lett.* **12** 2475–82

[10] Feser J P *et al* 2012 Thermal conductivity of silicon nanowire arrays with controlled roughness *J. Appl. Phys.* **112** 114306

[11] Nika D L, Pokatilov E P, Askerov A S and Balandin A A 2009 Phonon thermal conduction in graphene: role of Umklapp and edge roughness scattering *Phys. Rev.* B **79** 155413

[12] Bae M-H, Li Z, Aksamija Z, Martin P N, Xiong F, Ong Z-Y, Knezevic I and Pop E 2013 Ballistic to diffusive crossover of heat flow in graphene ribbons *Nat. Commun.* **4** 1734

[13] Maurer L N, Aksamija Z, Ramayya E B, Davoody A H and Knezevic I 2015 Universal features of phonon transport in nanowires with correlated surface roughness *Appl. Phys. Lett.* **106** 133108

[14] Hippalgaonkar K, Huang B, Chen R, Sawyer K, Ercius P and Majumdar A 2010 Fabrication of microdevices with integrated nanowires for investigating low-dimensional phonon transport *Nano Lett.* **10** 4341–8

[15] Oh J H, Shin M and Jang M-G 2012 Phonon thermal conductivity in silicon nanowires: the effects of surface roughness at low temperatures *J. Appl. Phys.* **111** 44304

[16] Alvarez F X, Jou D and Sellitto A 2011 Phonon boundary effects and thermal conductivity of rough concentric nanowires *J. Heat Transfer* **133** 022402

[17] Martin P, Aksamija Z, Pop E and Ravaioli U 2009 Impact of phonon-surface roughness scattering on thermal conductivity of thin Si nanowires *Phys. Rev. Lett.* **102** 125503

[18] Wei Z, Chen Y and Dames C 2012 Wave packet simulations of phonon boundary scattering at graphene edges *J. Appl. Phys.* **112** 24328

[19] Mazumder S and Majumdar A 2001 Monte Carlo study of phonon transport in solid thin films including dispersion and polarization *J. Heat Transfer* **123** 749–59

[20] Chen G 1998 Thermal conductivity and ballistic-phonon transport in the cross-plane direction of superlattices *Phys. Rev.* B **57** 14958–73

[21] Randrianalisoa J and Baillis D 2008 Monte Carlo simulation of steady-state microscale phonon heat transport *J. Heat Transfer* **130** 72404

[22] Péraud J P M and Hadjiconstantinou N G 2011 Efficient simulation of multidimensional phonon transport using energy-based variance-reduced Monte Carlo formulations *Phys. Rev.* B **84** 205331

[23] Lacroix D, Joulain K and Lemonnier D 2005 Monte Carlo transient phonon transport in silicon and germanium at nanoscales *Phys. Rev.* B **72** 64305

[24] Lacroix D, Joulain K, Terris D and Lemonnier D 2006 Monte Carlo simulation of phonon confinement in silicon nanostructures: application to the determination of the thermal conductivity of silicon nanowires *Appl. Phys. Lett.* **89** 103104

[25] Jean V, Fumeron S, Termentzidis K, Zianni X and Lacroix D 2015 Monte Carlo simulations of phonon transport in Si nanowires with constrictions *Int. J. Heat Mass Transfer* **86** 648–55

[26] Bera C 2012 Monte Carlo simulation of thermal conductivity of Si nanowire: an investigation on the phonon confinement effect on the thermal transport *J. Appl. Phys.* **112** 74323

[27] Chen Y, Li D, Lukes J R and Majumdar A 2005 Monte Carlo simulation of silicon nanowire thermal conductivity *J. Heat Transfer* **127** 1129–37

[28] Hao Q, Chen G and Jeng M-S 2009 Frequency-dependent Monte Carlo simulations of phonon transport in two-dimensional porous silicon with aligned pores *J. Appl. Phys.* **106** 114321

[29] Klitsner T, VanCleve J E, Fischer H E and Pohl R O 1988 Phonon radiative heat transfer and surface scattering *Phys. Rev.* B **38** 7576–94

[30] Moore A L and Shi L 2014 Emerging challenges and materials for thermal management of electronics *Mater. Today* **17** 163–74

[31] Boukai A I, Bunimovich Y, Tahir-Kheli J, Yu J-K, Goddard W A III and Heath J R 2008 Silicon nanowires as efficient thermoelectric materials *Nature* **451** 168–71

[32] Ramayya E, Maurer L, Davoody A and Knezevic I 2012 Thermoelectric properties of ultrathin silicon nanowires *Phys. Rev.* B **86** 115328

[33] Holland M G 1963 Analysis of lattice thermal conductivity *Phys. Rev.* **132** 2461–71

[34] Hurst W S and Frankl D R 1969 Thermal conductivity of silicon in the boundary scattering regime *Phys. Rev.* **186** 801–10

[35] Prasher R, Tong T and Majumdar A 2008 Approximate analytical models for phonon specific heat and ballistic thermal conductance of nanowires *Nano Lett.* **8** 99–103

[36] Soffer S B 1967 Statistical model for the size effect in electrical conduction *J. Appl. Phys.* **38** 1710

[37] Ziman J M 1960 *Electrons and Phonons (International Series of Monographs on Physics)* ed T Sugawara (Oxford: Oxford University Press)

[38] Maznev A A 2015 Boundary scattering of phonons: specularity of a randomly rough surface in the small-perturbation limit *Phys. Rev.* B **91** 134306

[39] Ramiere A, Amrit J and Volz S 2013 Role of boundary roughness on heat transport in mesoscopic silicon ribbons at low temperatures *NanoEnergy Lett.* **6** 13–4

[40] Blackstock D T 2000 *Fundamentals of Physical Acoustics* (New York: Wiley)

[41] Alaie S, Goettler D F, Su M, Leseman Z C, Reinke C M and El-Kady I 2015 Thermal transport in phononic crystals and the observation of coherent phonon scattering at room temperature *Nat. Commun.* **6** 7228